Computer Networks 220 (2023) 109504

Contents lists available at ScienceDirect

Computer Networks

journal homepage: www.elsevier.com/locate/comnet

Effect of the incident angle of a transmitting laser light on the coverage of a NLOS-FSO network

Paa Kwesi Esubonteng *, Roberto Rojas-Cessa

Networking Research Laboratory, Department of Electrical and Computer Engineering, New Jersey Institute of Technology, Newark, NJ, 07102, USA

ARTICLE INFO

Keywords:
Free-space optical communications
Optical wireless communications
Nondirect optical communications
Diffuse reflection
DR displacement
Lambertian diffusion

ABSTRACT

In this paper, we propose a model of the coverage and achievable data rates in No Line-of-Sight Free-Space Optical Communications (NLOS-FSOC) as a function of the angle of incidence. NLOS-FSOC uses diffuse reflected light to establish communication between two or more stations that are with or without line-of-sight to each other. Different from free-space optical communications (FSOC), NLOS-FSOC uses a diffuse reflector (DR) between a transmitter and a receiver so that LOS is not required between them but between the station and the DR. Unlike a mirror, the DR reflects the incident light to all directions but to itself and that reflection broadcast the optical channel to all receivers within LOS. The optical broadcast channel establishes a true optical local area network (OLAN). However, the reflected power and the coverage of an OLAN largely depend on the angle of incidence of transmitted laser beam. Therefore, the planning and building of an OLAN with NLOS-FSOC must consider this angle to optimize coverage, to set range, or to estimate the achievable communication data rates.

The proposed model and presented analysis center on an outdoor urban setting where mobile stations, represented by cars, travel through a city street. In such scenario, we estimate the average reflected power at the DR, the received power at different locations of the covered area, and their achievable communication data rates for downlink and uplink communications. With the consideration of mobile stations, we identify different displacement configurations that represent the different traveling paths of a mobile station with respect to a DR configuration on the urban scenario. Our extensive numerical evaluations on the different traveling and location scenarios show the effect that the incidence angle has on the coverage, the achievable data rates on an OLAN, and highlight the pros and cons of each different displacement. These results also show the options for the placement and orientation of the DR and ground optical base stations for an effective and extensive coverage and the signal quality of transmissions made by mobile stations traveling through the covered area in an NLOS-FSOC OLAN.

1. Introduction

Free space optical communications (FSOC) achieve higher data rates than radio frequency (RF) communications because of the operating frequencies of FSOC are in the light region of the spectrum [1–5]. FSOC is an attractive technology for short-, moderate-, and long-distance communications, and for its immunity to electromagnetic interference [6]. Applications of FSOC span from provisioning of basic Internet services [2,6–8], backhaul signaling for embedded systems [9], control signaling, data transfers in data centers [10,11], communications in high-speed trains [8,12–15], and unmanned aerial vehicles (UAVs) [2,16,17].

In FSOC, a transmitter modulates data over light and sends the signal to the receiver. The receiver demodulates the received light and recovers the data. FSOC requires a direct Line of Sight (LOS) between the transmitter and receiver and a rigorous beam alignment with the receiver [18–20]. This LOS requirement reduces the application scope of FSOC to point-to-point links, and in turn, to a small number of practical scenarios.

Fortunately, No-Line-of-Sight FSOC, or NLOS-FSOC for short, offers a method for communicating stations that have no LOS in between [21–25]. NLOS-FSOC uses a diffuse or Lambertian reflection (instead of a specular one) through a diffuse reflector (DR), to reflect laser light to every angle from the DR except towards itself [22,26]. The reflected light is detectable by stations with LOS to the DR and within the communications range. Such a broadcast channel gives place to an optical local area network (OLAN) [27,28].

NLOS-FSOC inherits many features of FSOC and, but more interestingly, it adds others not available in FSOC, such as a broadcast capability. NLOS-FSOC enables two or more stations communicate through a broadcast channel. This feature not only rids the LOS

* Corresponding author.
E-mail addresses: pae5@njit.edu (P.K. Esubonteng), rojas@njit.edu (R. Rojas-Cessa).

https://doi.org/10.1016/j.comnet.2022.109504
Received 2 February 2022; Received in revised form 18 November 2022; Accepted 29 November 2022
Available online 5 December 2022

requirement between a transmitter and receiver but it leverages the robustness of optical communications. With this feature, NLOS-FSOC resembles some broadcast properties of RF communications to some extent, and significantly increases the practicality of optical wireless communications. On the other hand, those features also require the consideration of multi-path dispersion and medium access control mechanisms in the operation of NLOS-FSOC. For instance, full duplex communication in NLOS-FSOC may use a single or multiple DRs, with one DR for an uplink and another for a downlink.

A transmitter may be placed far away from the DR but a receiver may not. In NLOS-FSOC, the received power at a station greatly depends on the distance from the DR to the station but also on the angle of incidence of the transmitted beam. This distance may be increased by selecting a suitable angle of incidence and that determines the optimal placement of a communicating station. The signal loses power with the square of the distance between the receiver and DR, and that loss limits the longest distance of a receiver from the DR. This angle of incidence determines the intensity of the reflected light and, therefore, the received power in each location of the covered area. Therefore, the effect of the angle of incidence on the power received by stations in the network is of interest.

The question that this paper aims to answer is: How is the received power affected by the transmissions from the different locations in the area of coverage? To answer this question, we model the received power as a function of the angle of incidence in this paper. With the proposed model, we show that while the angle of incidence remains constant for fixed ground base station and DR, it changes for a transmitting station that moves through the area of coverage and, in turn, the received power also changes for the receiving station, even if this station is stationary. To consider transmissions from and receptions at different locations in the covered area, we consider mobile stations, or cars, that travel through the area of coverage. The consideration of such mobile stations also lead us to develop three general displacement models for a flat DR and a flat covered area. These displacement models, or configurations set by the position and location of the DR in such an OLAN, determine how the receive power changes as a mobile station changes its location on the area of coverage. We analyze the relationship between the incidence angle of transmissions in the covered area for the considered configurations and the received power.

In this paper, we consider communications in an outdoor and urban scenario; modeled as a city street, that uses a DR for establishing a broadcast optical medium where mobile stations (e.g., cars) that access Internet communications through a ground optical base station (OBS). The DR in LOS of multiple mobile stations not only enables communications but also the transmission of large data rates that optical communications can achieve. The NLOS-FSOC framework is easy to deploy in urban and sub-urban settings as the infrastructure is mainly the installation of DRs while an OBS may be dedicated to a DR. The data rates of the considered setting range from 0.5–20 Gbps.

In summary, the contributions of this paper are: (1) The proposal of a model to compute the received power, the coverage, and the achievable data rates in an NLOS-FSOC OLAN as a function of the angle of incidence for a downlink and an uplink transmission, (2) we analyze the relationship between the reflected power, received power, data rates, and coverage, and (3) propose three general displacement models for mobile stations to determine how the data rates of a mobile station varies as it travels through the area of coverage for a downlink and uplink transmissions. Our model finds its use in the selection of the location of and positioning of a DR and OBS to achieve a suitable coverage and high data rates.

The remainder of this paper is organized as follows. Section 2 describes related works. Section 3 introduces the proposed framework and presents the analysis of the angle of incidence in NLOS-FSOC. Section 4 presents the effects of the incidence angle on the received power and the corresponding data rate for downlink and uplink transmissions of the NLOS-FSOC an OLAN through extensive numerical evaluations. Section 5 discusses the reduction of noise at the DR for outdoor use during daytime. Section 6 draws our conclusions.

2. Related works

To achieve data rates in 5G mobile communications for vehicular networks, several works have focused on improving the throughput of radio frequency technology in cellular networks [29–31]. Such a network approaches combine cloud computing, software defined networking, and fog cells to achieve data rates between 33 Mbps and 1 Gbps.

To achieve higher data rates, optical communications need to be considered. While FSOC can potentially achieve 1 Gbps and higher data rates, alignment is a usual impediment for mobile stations to achieve such communications. However, the use of diffuse reflections may relax such complexity. Diffuse reflections can be observed from many angles and that makes it different from specular reflections, which can only be seen from a single angle. Both specular and diffused reflected transmissions have been considered in the past [23,32–36]. Their use to improve and extend communication range has been addressed in optical networks [23,35] and in radio communications [32–34,36]. Masterson et al. [32] and Arun et al. [33] have suggested beamforming from reflected radiowaves as a technique to improve network throughput. This technique not only extends the range of the network but increases data rates. Those works consider the installation of reflective surfaces in parts of the network to reflect some of the energy from radiowaves towards specific regions with no LOS or where coverage is minimal or non-existent. Table 1 lists works that use active and passive reflective surfaces and the applications of such reflective surfaces. Passive reflectors use their physical properties to reflect the signal while active may use additional resources for the same goal. The table also shows that most works are based on specular reflections, and that only FSOC may be able to use diffuse reflection. The work in this paper falls in this last category.

In the light region of the spectrum, reflective capabilities of common materials, such as aluminum foil, polytetrafluoroethylene (PTFE) tape, and titanium dioxide paint, are used as a diffuse reflector in an NLOS-FSOC OLAN. Reflective screens enable simultaneous optical communications for multiple mobile stations without the use of multi-array LEDs directed towards multiple mobile stations in a network [37,38].

Several works have targeted modeling and analysis for indoor optical networks using an nondirect LOS technique [22,39–42]. While some works trace and model the path of light rays in an indoor environment, others suggest the use of an infra-red light source to transmit data and by focusing the transmitter's light on indoor walls and capturing the reflections from the wall by an optical receiver [22,41,42].

Studies have shown achievable data rates between 0.5–40 Gbps in point-to-point visible-light links for vehicular networks [43–48]. In such works, an LED is used as a transmitter and a camera as a receiver, which are fitted into a vehicle's headlight and taillight, respectively [45,46]. Several works have shown feasibility of direct LOS in vehicle-to-vehicle (V2V) optical communications with a noisy environment (e.g., rain, fog, and sunlight) [43,47,48].

Considering the high feasibility of optical links, Wilkins et al. [49] extended V2V communications infrastructure to fixtures (i.e., signposts, street lights, traffic lights) of the moving vehicle's surrounding environments. In this setup, an OT is attached to the fixture to support bi-directional LOS communication between the fixtures and the vehicle.

DRs in an optical network have been used to provide outdoor bi-directional communications between an OBS and a vehicle [23,50]. The framework used by Kaymak et al. [23] established an uplink and the corresponding downlink by placing DRs in the sight of the OT of mobile stations and an OBS. Their results showed achievable data rates between 0.3 and 1 Gbps. The configurations used compare the performance of the network when the DR is placed in front of a vehicle and on its side. Macaluso et al. [50] proposed the first MAC schemes for NLOS-FSOC for single and multiple projected beams. This work showed space–time trade-offs involved in such access schemes.

The proposed work in this paper fills the void on the modeling of the received power as a function of the angle of incidence. With this model, the achievable data rates of transmissions from different locations of an OLAN can be determined for a single and fixed DR.

Table 1
Communication technology and Type of reflective surface.

Technology	Surface	Reflection	Spectrum	Application
RF	Active	Specular	UHF	Programmable wireless and reflective radio [51], MIMO symbiotic networks [52], Communication over fading channel [53]
RF	Passive	Specular	UHF	Controlled distribution of WiFi signal indoor [54,55], Minimize the transmit power of WiFi access point [56]
NLOS-FSO	Passive	Specular	Visible, Infrared	Wavefront shaping using micromirror devices [57], Underwater FSOC using reflected light [58], Performance analysis of an NLOS-FSO system [59]
NLOS-FSO	Passive	Diffuse	Visible, Infrared	Improve transmission bandwidth for indoor FSOC [22], Internet access using diffused light [23], Beam selection on a diffuse reflector [50]

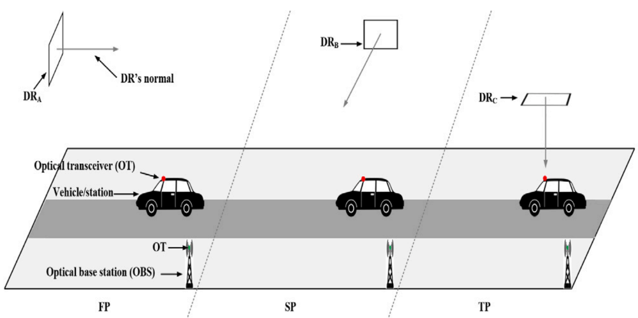

Fig. 1. Simplified diagram of the configuration of OLAN set up.

3. System configuration and model

The area of coverage of a DR describes locations where the receive power is large enough to be acquired by a receiver (or photodiode) and for a fixed OBS to receive the signal transmitted from different locations. While the range and boundaries of a downlink and uplink may be different in such an scenario, here we consider a city street. In such case, the area is limited by the dimensions of the street and the location and position of the DR. We describe the configuration and introduce the model of angle of incidence used to estimate reflected power, received power, and achievable data rates.

3.1. System configuration

Our framework focuses on the last-mile access infrastructure, used as backhaul Internet access for mobile and stationary stations. As a practical application example, and without losing generality, DRs and OBS are attached to existing infrastructures such as street light posts, traffic and sign posts, buildings, among others [49], and an stationary OBS connected to the last-mile access provides Internet access for the area of coverage.

The OBS provides a downlink response to uplink requests received from mobile stations in the area of coverage. Fig. 1 shows the FP configuration in an OLAN where the moving mobile station travels towards the DR (see DR_A). We call this as *front positioning configuration* (FPC). Similarly, the DR may be placed at the side of the road so that the mobile station travels with angle of 90 or 270° with the DR's normal (see DR_B), we call it *side positioning configuration* (SPC). The DR can also be positioned above the middle of the street, facing downwards, so that a mobile station travels underneath the DR in an angle also of 90 or 270° with the DR's normal (see DR_C), we call it a *top positioning configuration* (TPC).

In any of the configurations, the intensity of light from the reflecting surface varies as a cosine function of the angle between the incident light and the normal of the reflecting surface, as represented by:

$$I_r = I_0 cos\theta, \tag{1}$$

where I_r, I_0, and θ are the intensity of reflected light, the intensity of incident light, and the angle of incidence, respectively. The incident light may be transmitted by the OBS (*downlink*) or the mobile stations (*uplink*) as here we consider that any communications (mobile-to-mobile or Internet-to-mobile) uses the OBS.

Mobile stations communicating with the OBS direct their OTs toward the current DR for uplink and downlink. These mobile stations must be ATP capable to maintain LOS to the DR. The mobile stations use two OTs to enable seamless handover between two DRs; the communicating and the handover OT. The communicating OT transmits and receives data, and the handover OT acquires, tracks, and points to the next DR in the traveling path of the mobile station. The OBS has an OT pointed and dedicated to the DR at which it transmits a laser beam as a downlink transmission. The OBS also receive the reflected light from the transmissions of a mobile station, as an uplink transmission.

Using a beacon signal, the mobile stations align their OTs to the DR for uplink transmissions [60,61]. The beacon device is attached to the top center of the DR, and the OBS and mobile stations point their OTs to the DR. Because the OBS and the DR are fixed, the OTs of the OBS are pointed to the surface of the DR during installation. The wavelength of the proposed beacon signal is 976 nm [61].

3.2. System model

Table 2 shows the terms and notations used in this paper. We model the uplink but the model can be directly applied on the downlink. By Lambertian law on atmospheric transmission [62], the intensity (I_0) of the incident light at a distance can be expressed as:

$$I_0 = I_t\ e^{-\gamma d}, \tag{2}$$

where I_t is the optical intensity of transmitted light, γ is the extinction coefficient that accounts for the deterioration of I_t as a result of the absorption and scattering in the atmosphere, and d is the distance, in km (i.e., the distance between transmitter and surface of DR). While absorption due to water or water vapor affects most wavelengths between 1300–1400 nm, the absorption due to atmospheric gases varies for different wavelengths, except for 650 nm [63]. Scattering may result from aerosol, smoke, or weather conditions such as fog, snow, and clouds [63,64]. Here, γ, in dB/km is computed for different atmospheric conditions using Kim's model [65]:

$$\gamma = (\frac{3.91}{v})(\frac{\lambda}{550})^{-q}, \tag{3}$$

where v is the visibility range in km, λ is the wavelength, in nm, and q is the size distribution of the scattering particles, or:

$$q = \begin{cases} 1.6, & \text{high visibility } (v > 50) \text{ km} \\ 1.3, & \text{average visibility } (6 < v \le 50) \text{ km} \\ 0.16v + 0.34, & \text{hazy visibility } (1 < v \le 6) \text{ km} \\ v\ - 0.5, & \text{mist visibility } (0.5 < v \le 1) \text{ km} \\ 0, & \text{fog visibility } (0.01 < v \le 0.5) \text{ km} \end{cases} \tag{4}$$

Because the DR is a Lambertian surface, the reflected light is calculated using the Lambert's cosine law on θ, where θ is the angle between the normal of the DR to the point of incidence of the light, or angle of incidence. The law states that "the intensity varies as the cosine of

Table 2
Notations used in this paper.

Notation	Description
P_t	Transmit power
P_0	Incident power
P_r	Reflected power
P	Received power
B	Data rate
d_0	Travel distance
o	Horizontal distance
h	Vertical distance
θ	Angle of incidence

the angle incident of the light upon the object viewed" [62], and this expression is given in (1).

Lambert's law also states that "the intensity of light is inversely proportional to the square of the distance of the observer to the source [62]". Hence the intensity of light received by an observer (mobile station or OBS) at a distance d from the DR can be expressed as:

$$I = \frac{I_r}{d^2\pi} \implies I = \frac{I_0 cos\theta}{d^2\pi} \tag{5}$$

Considering the reflectance of the material used as the DR into (5), the expression for I becomes:

$$I = \frac{I_0 R cos\theta}{d^2\pi} \tag{6}$$

In our OLAN, a mobile station and OBS transmit a narrow laser beam, with a width of 1 mrad, onto the DR, and the area of the projected beam on the DR is denoted as S_t and its size is a function of the distance between the transmitter and the DR. Likewise, the mobile station and OBS receive the reflected transmissions from the surface of the DR, at where the lens of the OT is focused. The size of the area the lens of the receiver focuses (S_r) depends on the aperture area A_r of the photodiode lens and d_r, or:

$$S_r = \frac{A_r\ d_r}{f_r\ cos\ \theta_r}, \tag{7}$$

where f_r is the focal length of the lens and θ_r is the angle between the normal of the DR and the LOS from the center of the lens [39]. The area of the region $d\sigma$ where S_t and S_r intersect is critical in establishing the strength of the communication link, or:

$$I = \int_{S_t \cap S_r} \frac{I_0 R cos\theta A_r}{S_t d^2\pi} d\sigma \tag{8}$$

Because the intensity of the transmitted beam also depends on the beam's diameter, the use of a narrow laser beam for transmissions makes S_t of the transmitter be smaller than the S_r at the receiver (i.e., $S_t \ll S_r$). The photodiode used by the receiver has $A_r \ll d$ [23,39,50]. Hence, the reflected power P_r and received power P become:

$$P_r = P_t\ e^{\gamma d} R cos\theta \tag{9}$$

and

$$P = \frac{P_r A_r}{d^2\pi} \tag{10}$$

The received power in (10) is a function of P_t, γ, R, θ, A_r and d. The factors P_t and A_r depend on the laser diode and photodiode. Therefore, they are considered and designed during the manufacturing process of the OT. While a large P_t and A_r increase the value of P, the largest P_t is limited by eye safety, and the A_r of an OT is designed to be portable to ease usage.

In high visibility weather, the attenuation loss due to γ is < 0.2 dB/km for wavelengths between 780 and 1600 nm [66]. Hence, it is considered negligible for the scope of this paper. Also, R of many common materials has been tested and found to be $\cong 1$ [27,28,67]. Such value simplifies the selection of a DR for NLOS-FSOC. However, θ and d depend on the location of the transmitter. Here, d significantly affects P, and θ of the transmitted beam varies with the direction of travel of the transmitting mobile station. P_r and P are then significantly affected by θ. Consequently, P_r determines the suitable displacement model in an OLAN, the size of the handover region, the data rate, and size of the area of coverage. We consider the channel to be solely affected by atmospheric attenuation in our analysis. The pointing errors between the receiver and DR are considered negligible because of the large surface of the DR on which the OT focuses. We assume the transmission from the users always fall on the DR. Therefore, pointing errors are not significant for transmissions aimed at the DR.

3.3. Estimation of the angle of incidence (θ)

The angle of incidence determines whether there is partial or no reflected signal. A transmission with $\theta = 0°$, $30°$, $60°$, or $90°$ achieves 100, 86.7, 50, or 0% reflection, respectively. Mobile stations with $\theta \geq 90°$ have no LOS with the DR and receive no reflected light, whereas all other mobile transmissions for which $\theta < 90°$ receive a fraction of the reflected light. Here, d varies as the mobile station travels. The value of θ and d are considered according to the location of the DR, mainly by the height difference between those of the mobile station's OT and the DR's (vertical distance h), the parallel distance between the DR, and the mobile station's OT (horizontal distance o), and d_0. Figs. 2(a), 2(b), and 2(c) show these distances for a FPC, SPC and TPC, respectively. We use these distances to estimate θ of an NLOS-FSOC uplink and downlink.

A (−) sign before d_0, or $-d_0$, indicates that the mobile station is located after the center of the DR (i.e., to the left of the DR). Otherwise, the mobile station is located before the center of the DR (i.e., to the right of the DR).

Here, θ in Fig. 2 is computed by the cosine rule as:

$$\theta = arccos(\frac{d_0^2 + d^2 - i^2}{2 d_0 d}), \quad d_0 \neq 0,\ d \neq 0 \tag{11}$$

for FPC,

$$\theta = arccos(\frac{o^2 + d^2 - i^2}{2od}), \quad o \neq 0,\ d \neq 0 \tag{12}$$

for SPC and

$$\theta = arccos(\frac{h^2 + d^2 - i^2}{2hd}), \quad h \neq 0,\ d \neq 0 \tag{13}$$

for TPC.

In these figures, the angles are $\angle EOA = \angle OAB = \angle ABC = 90°$. The line segment $\overline{OE} = \overline{AB}$ in FPC, the segment $\overline{OE} = \overline{BC}$ in SPC, and the segment $\overline{OE} = \overline{OA}$ in TPC.

For any of the configurations, when a mobile station has no LOS to the DR, $\theta = 90°$ or (i)–(iii). in (14). Also, communications is not possible for NLOS-FSOC when the mobile stations OT is close enough to touch the DR or (iv). in (14). The OTs with no LoS to the DR are out of the covered area of the OLAN, so they are not considered. However, the area of coverage can be extended by adding more DRs and are defined as an additional covered area, or by modifying the orientation of the DR.

$$\theta = \begin{cases} (i)\ 90°, & d_0 = 0 \text{ in FPC} \\ (ii)\ 90°, & o = 0 \text{ in SPC} \\ (iii)\ 90°, & h = 0 \text{ in TPC} \\ (iv)\ undefined, & d = 0 \text{ in all the configurations} \end{cases} \tag{14}$$

While d is common to any configuration, i depends on the displacement configuration. For example, d is determined as:

$$\overline{OC} = \sqrt{\overline{AB}^2 + \overline{BC}^2 + \overline{AO}^2} \quad or \quad d = \sqrt{d_0^2 + o^2 + h^2} \tag{15}$$

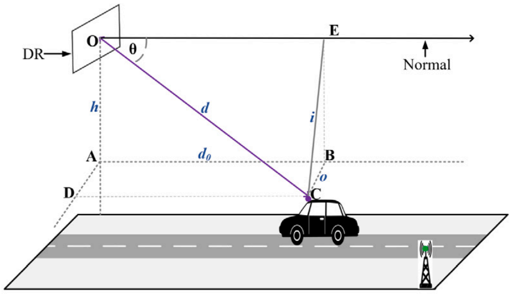

(a) Front positioning configuration (FPC).

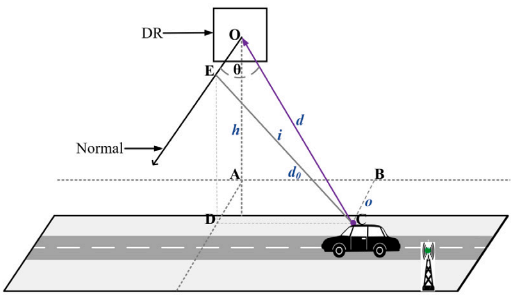

(b) Side positioning configuration (SPC).

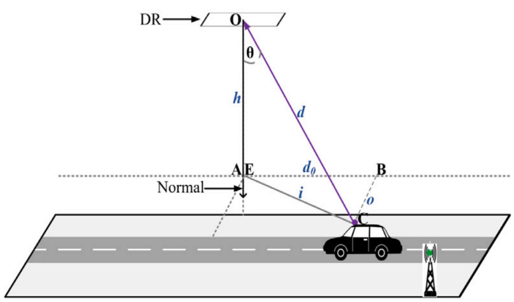

(c) Top positioning configuration (TPC).

Fig. 2. Positioning of the DR in the different displacement configurations.

and i is computed as:

$$\overline{CE} = \sqrt{\overline{BC}^2 + \overline{AO}^2} \quad or \quad i = \sqrt{o^2 + h^2} \tag{16}$$

for FPC,

$$\overline{CE} = \sqrt{\overline{AB}^2 + \overline{AO}^2} \quad or \quad i = \sqrt{d_0^2 + h^2} \tag{17}$$

for SPC, and

$$\overline{CE} = \sqrt{\overline{AB}^2 + \overline{BC}^2} \quad or \quad i = \sqrt{d_0^2 + o^2} \tag{18}$$

for TPC.

4. Model evaluations and results

Let us examine the parameters θ, P_r, and P for the road layout shown in Fig. 3, as an example. The curb's width of this road is 2 m

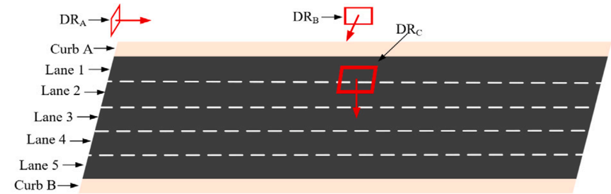

Fig. 3. Layout of a road with five lanes as area of coverage.

and each lane is 4-m wide. In the configuration, $h = 1$ m between the DR and an OBS and $h = 2$ m between the DR and a mobile station. The DR provides coverage for an area of size $\{d_0 \times o\} = \{200 \times 20\}$ m^2. We consider that a mobile station travels along the center of each lane on the road, or $o = \{4, 8, 12, 16, 20\}$ m for lanes 1 to 5, respectively. Also, the DR is placed at location $\{d_0, o\} = \{0, 0\}$ m for FPC and SPC, and $\{d_0, o\} = \{0, 12\}$ m for TPC. The DR in FPC provides coverage for $0 < d_0 \leq 200$ m, whereas the DR in SPC and TPC provide coverage for $-100 \leq d_0 \leq 100$ m. The OBS is placed along the ends of curb A (i.e., $o = 0$ m) or B (i.e., $o = 24$ m) so that the DR does not interfere with the vehicles traveling along the road. We consider that the OBS and mobile station transmit with $P_t = 50$ mW for a 1550 nm wavelength and under clear weather. The DR considered in this computation has a perfect diffuse reflectance (i.e., $R = 1$).

4.1. Downlink

4.1.1. Angle of incidence for downlink transmissions

The OBS for a FPC and TPC might be placed on either curb A or B from where it projects its beam on the DR. However, the OBS in the FPC has to be placed in front of the DR, that is, $d_0 > 0$ m in curb A to ensure communication, as stated in case (iv) of (14). The OBS in an SPC is placed along curb B only because there is no LOS to the DR in curb, or case (ii) of (14).

We compute θ for downlink transmissions from the OBS along the curb as a function of d_0 to determine the d_0 for which θ is the smallest and P_r is the largest. Fig. 4(a) shows θ for downlink transmissions. The graph shows that as d_0 increases, θ decreases in FPC, and it increases in both SPC and TPC. Fig. 4(b) shows P_r in the downlink according to (9) on Fig. 4(a). From the two graphs, we observe that a small θ produces a large P_r and vice versa. FPC produces the largest P_r along curb A because θ is small along this curb. P_r on curb A and B are identical for TPC. Therefore the DR can be placed at either curb. A large downlink P_r produces strong P at a mobile station receiving the transmission from the OBS. Therefore, the location of the OBS along the curb is chosen so that P_r is maximum. The OBS is placed at $d_0 = 10$ m on curb A for FPC and $d_0 = 0$ m on curb B for both SPC and TPC in the proposed layout.

4.1.2. Receive power and data rate

The downlink P and the corresponding B received by the stations across the area of coverage are computed for each configuration. We consider that the receiver is a Mercury Cadmium Telluride (HgCdTe) avalanche photodiode (APD) with high sensitivity to wavelengths at 1550 nm, as in [23]. The targeted minimum bit error rate (BER) is 10^{-9} for a link with a 15.56 dB signal-to-noise ratio (SNR). The receiver responsivity is 0.8 A/W and the aperture for the receiving lens is 9.5×10^{-3} m^2. The required number of photons is at least 57 to achieve a BER of 10^{-9} for SNR = 15.56 dB. The modulation scheme considered is On-Off-Keying-NonReturn-to-Zero (OOK-NRZ).

The graphs in Figs. 5(a), 5(b), and 5(c) show the received power for FPC, SPC, and TPC, respectively. In the graphs, P decreases as d_0 and o increase (i.e., an increase in d) between the DR and the vehicles OT. The largest and smallest P occur in SPC and TPC, respectively.

Here, data rate B is defined in terms of P as

$$P = \frac{N_p \hbar c B}{\lambda}, \tag{19}$$

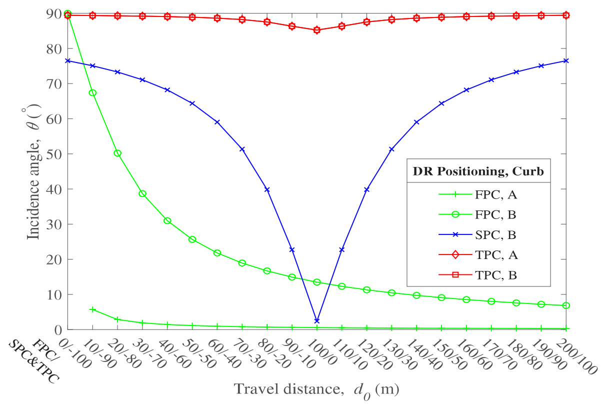

(a) Incidence angle θ as a function of d_0 for all three configurations.

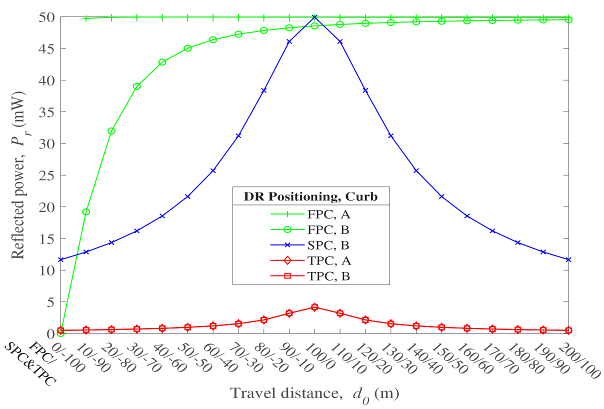

(b) Reflected power P_r as a function of d_0 for all three configurations.

Fig. 4. Graph of θ and P_r as a function d_0 for the downlink.

Table 3
Table showing P and corresponding B.

P (dBm)	<51.4	54.42	−51.4	−44.4	−41.4	−38.4
B (Gbps)	0	0.5	1	5	10	20

in the considered configurations, where N_p is the average number of photons for a single information bit, $\hbar$ is Planck's constant, and c is the speed of light. Table 3 shows the received power and the corresponding achievable data rates.

Figs. 6(a), 6(b), and 6(c) show the data rates of the road layout for FPC, SPC and TPC, respectively. These figures show the data rates as a representation of P across the area of coverage, using Table 3. The decline in data rates in the graphs is caused by the decline in P as d increases. This result implies that for a fixed h, B decreases as o, d_0, or both increase. The graphs show the smallest B is 0.5, 1, and 0 Gbps for FPC, SPC, and TPC, respectively. The smallest coverage in TPC is the result of a large θ when the OBS transmits, and that produces a small P_r and P across the area of coverage. On the other hand, the small θ in both FPC and SPC produces a large P_r and P. The centered location of the DR in SPC provides a higher data rate at the farthest locations of the covered area than those locations in FPC. The difference in data rates occurs because the largest d_0 in SPC is half the largest d_0 in FPC.

4.2. Uplink

The uplink transmission of the NLOS-FSOC is affected by the location of the transmitting vehicle as it travels on the covered area. Here, θ of a transmission by a mobile station is a function of d_0 and the center of the lane on which the vehicle travels. The value of θ across the area of coverage affects the uplink P_r, P, and B received at the OBS.

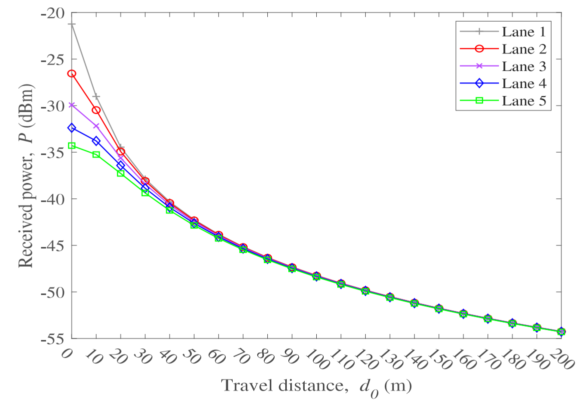

(a) Receive power P in dBm as a function of d_0 in FPC.

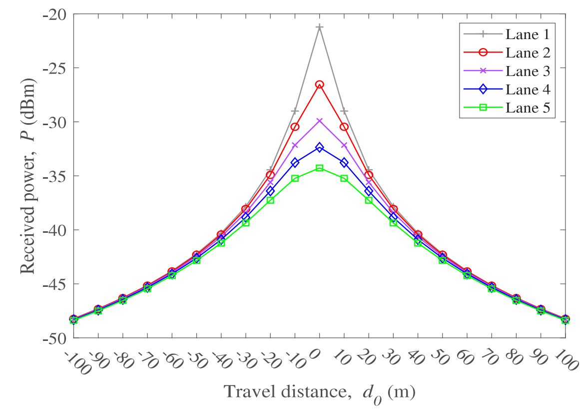

(b) Receive power P in dBm as a function of d_0 in SPC.

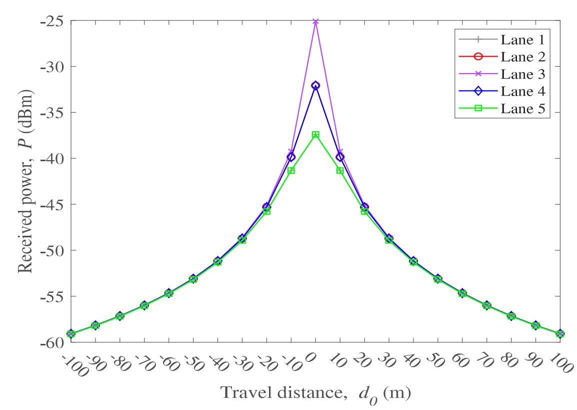

(c) Receive power P in dBm as as a function of d_0 in TPC.

Fig. 5. Receive power P as a function of d_0 for the downlink.

4.2.1. Angle of incidence for uplink transmissions

We estimate θ of the uplink as a function of d_0 of a vehicle traveling on the street as it transmits its beam onto the DR. Fig. 7(a) shows that θ decreases as d_0 increases, and that it also slightly increases for the farthest lanes from the DR (i.e., increased o) for FPC. Conversely, θ increases as d_0 increases for SPC. The lanes farther from the DR show that as o increases, θ slightly decreases, as shown in Fig. 7(b). Fig. 7(c) shows that θ increases as d_0 increases. The results show that θ for Lanes 1 and 5, and Lanes 2 and 4 are identical. Mobile stations traveling on lanes farther from the DR experience an increase in θ as o increases in TPC. The parameters that produce a significant decrease in θ for FPC and SPC are d_0 and o, respectively, whereas an increase in either

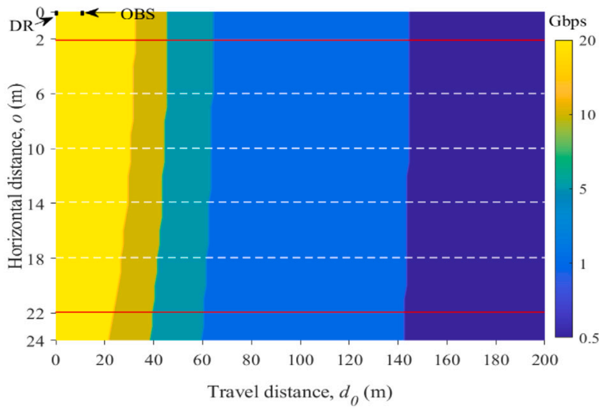

(a) Data rate in FPC.

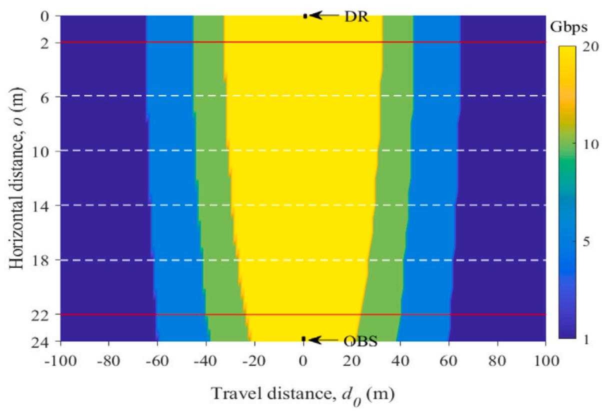

(b) Data rate in SPC.

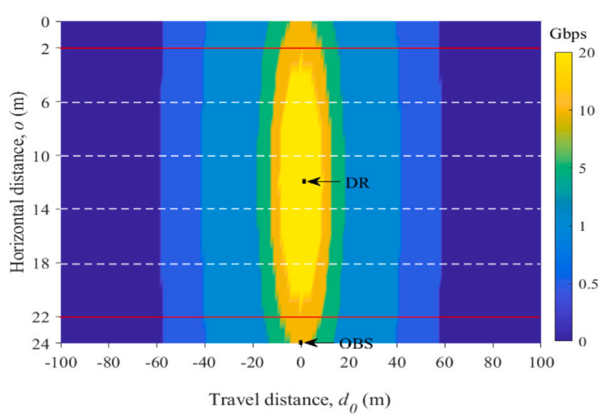

(c) Data rate in TPC.

Fig. 6. Data rate B as a function of d_0 and o.

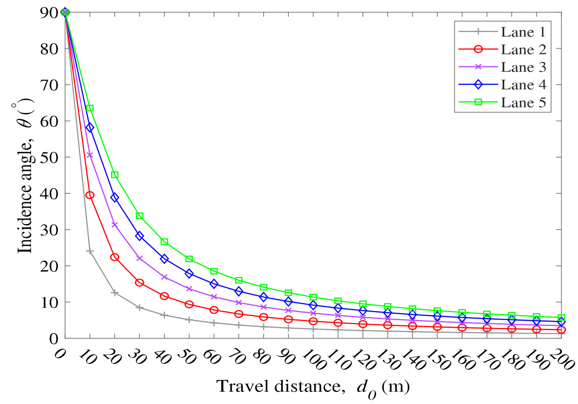

(a) Angle of incidence $\theta°$ for the lanes of a road in a FPC.

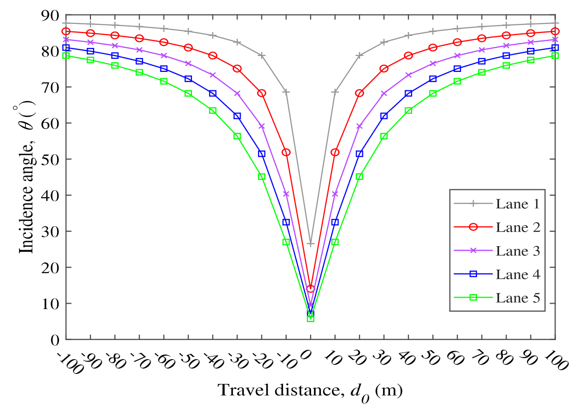

(b) Angle of incidence $\theta°$ for the lanes of a road in a SPC.

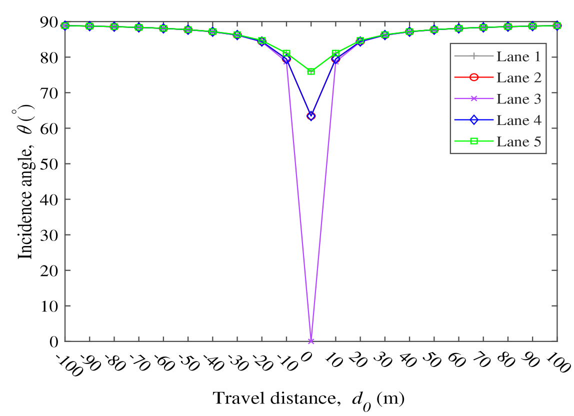

(c) Angle of incidence $\theta°$ for the lanes of a road in a TPC.

Fig. 7. Angle of incidence θ for the uplink on the considered road layout.

d_0, o, or both increases θ in TPC. From the Eqs. (11)–(13) used in the estimation of θ, increasing the parameters d_0, o and h, produce a decrease in θ for FPC, SPC, and TPC, respectively. This decrease of θ determines the scenarios for deploying such a configuration. For instance, a TPC is the preferred configuration in a setup where h is the largest parameter, such as a DR attached to a drone that provides coverage for a small compound.

4.2.2. Reflected power

Fig. 8 shows the uplink P_r corresponding to θ in Fig. 7 for the considered configurations. As shown in Fig. 8(a), more than 95% lanes in FPC achieve $P_r \geq 25$ mW whereas at most 25% and 2% of the covered area in SPC and TPC, respectively, achieve such P_r, as shown in Fig. 8(b) for SPC and Fig. 8(c) for TPC. The graphs show that the locations on the lanes that achieve a small θ also achieve a large P_r for the configurations, as expected.

4.2.3. Received power and data rate

Fig. 9 shows the computed uplink P at the OBS using the uplink P_r in Fig. 8. The graph shows that P is significantly affected by P_r in each configuration because d between the OBS and DR is fixed (i.e., d_0, o, and h of the OBS are fixed). Here, d contributes a constant loss in the uplink P. The smallest and largest losses in the uplink P occur in FPC and SPC, respectively. Together, the loss caused by d and the uplink P_r affect P, which in turn affects the uplink B. Because of the different uplink P at the different places of the lanes, the minimum uplink B

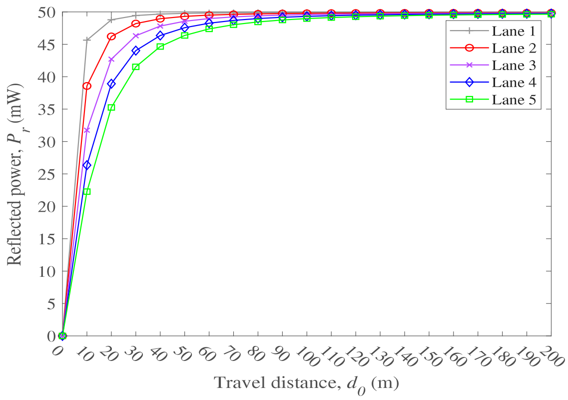

(a) The reflected power P_r in FPC

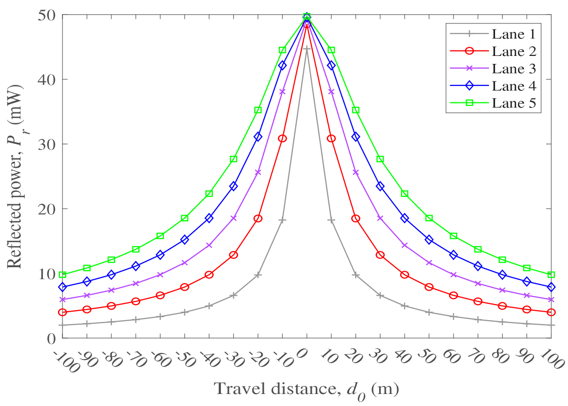

(b) Reflected power P_r in SPC.

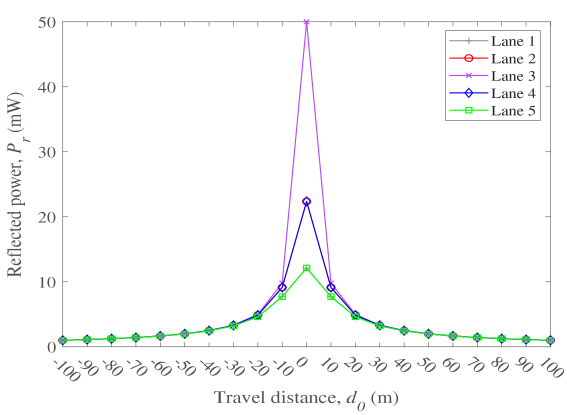

(c) Reflected power P_r in TPC.

Fig. 8. The Reflected power P_r for the uplink on the considered road layout.

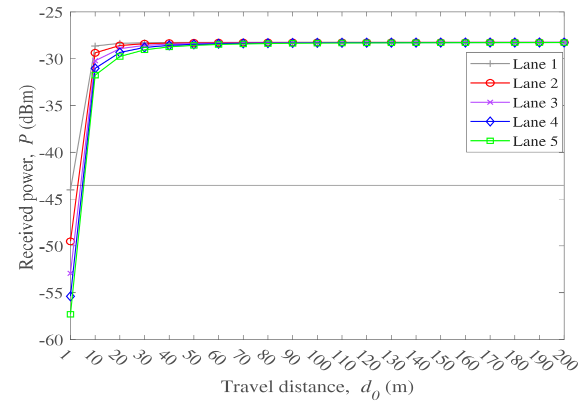

(a) Received power P in FPC.

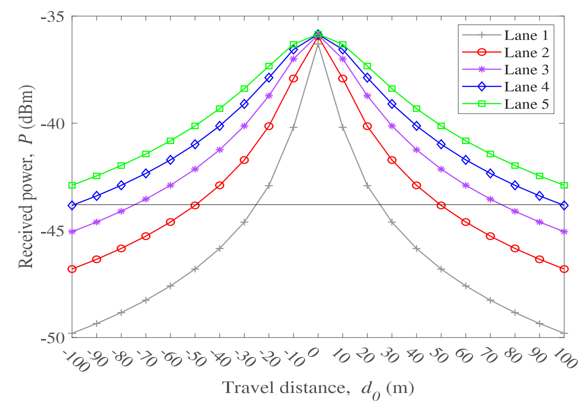

(b) Received power P in SPC.

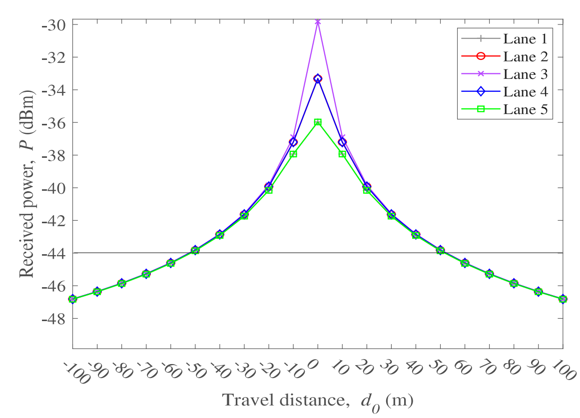

(c) Received power P in TPC.

Fig. 9. The Received power P at the OBS for the uplink.

may not be achieved at some regions of the road. For instance, for a minimum uplink B of 5 Gbps, which requires an uplink $P \geq -44.4$ dBm at the OBS, at least 95% of the transmissions along the lanes can achieve this data rate in FPC, as shown in Fig. 9(a). The region above the black line on the graph is the region where the transmission of a mobile station equals or exceeds −44.4 dBm. SPC and TPC have at least 70% and 60% of the transmissions along the lanes with uplink $P \geq -44.4$ dBm, as shown in Figs. 9(b) and 9(c), respectively.

On the other hand, for a minimum uplink B of 1 Gbps which requires an uplink $P \geq 51.4$ dBm, all the transmissions along the lanes in SPC and TPC are able to achieve this data rate except for FPC, where some of the transmissions from mobile stations at $d_0 < 2$ m produce a large θ and $P < -51.4$ dBm. Therefore, the uplink outage regions in any of the configurations are the locations on the lanes where the uplink P are so low that the minimum uplink B cannot be achieved. An example is the region below the black line in the graphs of Fig. 9 where the minimum uplink $B = 5$ Gbps. The largest and smallest B occur in FPC.

The largest uplink B can be achieved in FPC as shown in Fig. 9, because a large section of the road layout in this configuration has a small θ along the lanes (i.e., $d_0 > 30$ m), and this produces a large uplink P and B in the section. This advantage makes FPC the preferred configuration for uplink. The large section of the road with large uplink P reduces the uplink outage region in FPC. Also, the large uplink B in FPC, implies a large aggregated uplink B at the OBS. For a large area of coverage, fewer OBSs and DRs are required in the FPC as compared to the other configurations. The downlink coverage for FPC and SPC

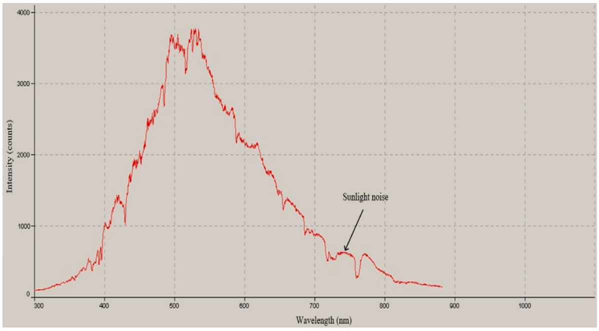

(a) Reflection from an unshaded DR.

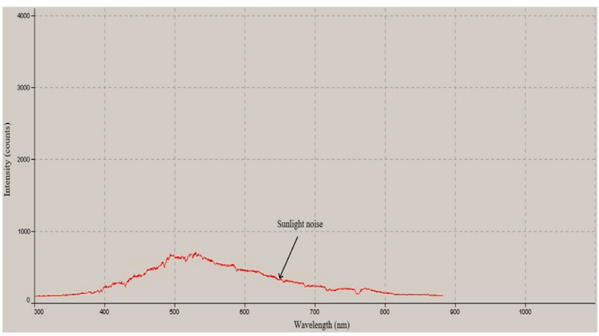

(b) Reflection from a shaded DR.

Fig. 10. Difference in noise floor between a shaded and unshaded DR.

are almost identical for a given distance from the DR, Therefore, FPC is most suitable configuration for vehicular communications on a road.

5. Sunlight noise in outdoor environments

NLOS-FSOC still faces many challenges to make it feasible for deployment. Some of those are using receivers sensitive enough and noise. In outdoor scenarios, sun radiation is a major source of noise. Fortunately, there are different well-known techniques to diminish such noise: filters [68], casing, and shading (awning). Being the last the simplest technique, we experimentally look into the spectrum observed in the reflected light on paper, used as a diffuse reflector.

We recorded the spectrum of the reflected light with direct sun illumination and another with shaded DR (i.e., without direct sunlight) to show the effectiveness of shading at midday of a sunny day. Fig. 10(a) shows the spectrum detected on the exposed DR, i.e., without a shade. The spectrum shows significant reflected light from the DR, even without a transmitted light beam. This reflected light represents the noise in the covered area of the optical network. In contrast, a shade significantly reduces the noise in the covered area of the optical network, as Fig. 10(b) shows. Other techniques can be also used for additional signal recovery [69]. In addition and overall, these figures also show that the selection of a wavelength in a less noisy region of the spectrum may simplify the noise filtering process.

6. Conclusions

In this paper, we proposed a model of reflected and received power as a function of the angle of incidence for a downlink and an uplink communication in NLOS-FSOC framework of an optical local area network in a vehicular communications scenario. This scenario considers ground-to-vehicle and vehicle-to-ground This scenario considers. Contrary to conventional free-space optical communications, NLOS-FSOC enables a broadcast channel where all stations transmit or receive data. We analyzed the effect that the angle of incidence of the incoming light beam has on the reflected power and received power in a scenario where communicating mobile stations travel along a city road. We considered three positioning configurations of the diffuse reflectors according to the traveling path of the vehicles. We analyzed the angle of incidence of the downlink where the transmitter is a fixed ground station and the uplink where the transmitters are the traveling vehicles.

Our analysis of the effect of the angle of incidence across the considered road layout for the downlink and uplink showed the significant parameters in each configurations. Deploying the appropriate configuration can help to provide a high data rate in the area of coverage. In the considered road layout, FPC provides a minimum downlink data rate of 0.5 Gbps in the covered area and guarantees an uplink data rate of 5 Gbps for distances greater than 2 m from the diffuse reflector. SPC provides the largest downlink data rate of 1 Gbps because of position of DR in the covered area and guarantees an uplink data rate of 5 Gbps for a maximum distance of 28 m from the DR when considering the lane with the weakest uplink P. TPC provides a downlink of 0.5 Gbps at a maximum distance of 58 m from the DR and guarantees an uplink data rate of 5 Gbps for a maximum distance of 55 m from the DR when considering the lane with the weakest uplink P.

The remaining challenges of the proposed approach are the design of medium access control schemes for efficiently using the features of a diffuse reflector and to enhance the size of the areas that are covered with enough light intensity to enable the highest data rates.

CRediT authorship contribution statement

Paa Kwesi Esubonteng: Conception and design of study, Acquisition of data, Analysis and/or interpretation of data, Writing – original draft, Writing – review & editing. **Roberto Rojas-Cessa:** Conception and design of study, Acquisition of data, Analysis and/or interpretation of data, Writing – original draft, Writing – review & editing.

Declaration of competing interest

The authors declare that they have no known competing financial interests or personal relationships that could have appeared to influence the work reported in this paper.

Data availability

No data was used for the research described in the article.

Acknowledgment

All authors approved the version of the manuscript to be published.

References

[1] V. Kukshya, H. Izadpanah, High-speed optical wireless connectivity: design challenges and performance evaluation, in: Optical Transmission Systems and Equipment for WDM Networking, Vol. 4872, International Society for Optics and Photonics, 2002, pp. 343–353.

[2] M.K. Al-Akkoumi, R.C. Huck, J.J. Sluss Jr., High-speed communications enabling real-time video for battlefield commanders using tracked FSO, in: Atmospheric Propagation IV, Vol. 6551, International Society for Optics and Photonics, 2007, 655105.

[3] K. Wang, A. Nirmalathas, C. Lim, E. Skafidas, K. Alameh, Free-space optics for high-speed reconfigurable card-to-card optical interconnects, in: Nonimaging Optics: Efficient Design for Illumination and Solar Concentration X, Vol. 8834, International Society for Optics and Photonics, 2013, p. 88340I.

[4] R. Slomski, E. Skedek, Optical communication as a perspective method of exchanging data in dedicated systems, in: Photonics Applications in Astronomy, Communications, Industry, and High-Energy Physics Experiments 2014, Vol. 9290, International Society for Optics and Photonics, 2014, p. 92900C.

[5] J.C. Juarez, K.T. Souza, N.G. Bos, A.M. Brown, B.M. Cannon, K.G. Petrillo, J.L. Riggins II, J.E. Sluz, H.J. Tomey, R.A. Venkat, Lasercomm system development for high-bandwidth terrestrial communications, in: Atmospheric Propagation XIII, Vol. 9833, International Society for Optics and Photonics, 2016, p. 98330A.
[6] H.H. Refai, J.J. Sluss Jr., H.H. Refai, M. Atiquzzaman, Transporting RF signals over free-space optical links, in: Free-Space Laser Communication Technologies XVII, Vol. 5712, International Society for Optics and Photonics, 2005, pp. 46–54.
[7] K.A. Morrison, COTS low-cost 622-Mb/s free-space laser communications link for short-distance commercial applications, in: Free-Space Laser Communication Technologies XII, Vol. 3932, International Society for Optics and Photonics, 2000, pp. 52–59.
[8] O.B. Karimi, J. Liu, C. Wang, Seamless wireless connectivity for multimedia services in high speed trains, IEEE J. Sel. Areas Commun. 30 (4) (2012) 729–739.
[9] J.Y. Hui, Wireless optical ad-hoc networks for embedded systems, in: Conference Proceedings of the 2001 IEEE International Performance, Computing, and Communications Conference (Cat. No. 01CH37210), IEEE, 2001, pp. 140–144.
[10] N. Hamedazimi, Z. Qazi, H. Gupta, V. Sekar, S.R. Das, J.P. Longtin, H. Shah, A. Tanwer, Firefly: A reconfigurable wireless data center fabric using free-space optics, in: Proceedings of the 2014 ACM Conference on SIGCOMM, 2014, pp. 319–330.
[11] Z. Ghassemlooy, H. Le-Minh, Application of free-space optics in future data centers (Conference presentation), in: Broadband Access Communication Technologies XIII, Vol. 10945, International Society for Optics and Photonics, 2019, p. 109450L.
[12] T. Arita, F. Teraoka, Providing a high-speed train with a broadband NEMO environment: A report of a field test using a train in service, in: Proceedings of the Sixth Asian Internet Engineering Conference, 2010, pp. 64–71.
[13] H. Urabe, S. Haruyama, T. Shogenji, S. Ishikawa, M. Hiruta, F. Teraoka, T. Arita, H. Matsubara, S. Nakagawa, High data rate ground-to-train free-space optical communication system, Opt. Eng. 51 (3) (2012) 031204.
[14] S. Fathi-Kazerooni, Y. Kaymak, R. Rojas-Cessa, J. Feng, N. Ansari, M. Zhou, T. Zhang, Optimal positioning of ground base stations in free-space optical communications for high-speed trains, IEEE Trans. Intell. Transp. Syst. 19 (6) (2017) 1940–1949.
[15] Y. Kaymak, S. Fathi-Kazerooni, R. Rojas-Cessa, J. Feng, N. Ansari, M. Zhou, T. Zhang, Beam with adaptive divergence angle in free-space optical communications for high-speed trains, 2018, arXiv preprint arXiv:1812.11233.
[16] G.C. Gilbreath, W.S. Rabinovich, T.J. Meehan, M.J. Vilcheck, R. Mahon, R. Burris, M.F. Stell, I. Sokolsky, J.A. Vasquez, C.S. Bovais, et al., Large-aperture multiple quantum well modulating retroreflector for free-space optical data transfer on unmanned aerial vehicles, Opt. Eng. 40 (7) (2001) 1348–1357.
[17] A. Harris, J.J. Sluss Jr., H.H. Refai, P.G. LoPresti, Atmospheric turbulence effects on a wavelength diversified ground-to-UAV FSO link, in: Free-Space Laser Communication Technologies XVIII, Vol. 6105, International Society for Optics and Photonics, 2006, p. 61050S.
[18] H. Zhang, H. Li, X. Dongya, C. Chao, Performance analysis of different modulation techniques for free-space optical communication system, TELKOMNIKA (Telecommun. Comput. Electron. Control) 13 (2015) 880.
[19] A. Malik, P. Singh, Free space optics: current applications and future challenges, Int. J. Opt. 2015 (2015).
[20] A.E. Willner, C. Liu, Perspective on using multiple orbital-angular-momentum beams for enhanced capacity in free-space optical communication links, Nanophotonics 10 (1) (2021) 225–233.
[21] O. Bouchet, H. Sizun, C. Boisrobert, F. Fornel, P.-N. Favennec, Free-space optics: Propagation and communication, Free-Space Opt.: Propag. Commun. (2010) http://dx.doi.org/10.1002/9780470612095.
[22] D. Wu, Z. Ghassemlooy, S. Rajbhandari, H. Le Minh, A.C. Boucouvalas, Improvement of transmission bandwidth for indoor optical wireless communication systems using an elliptical Lambertian beam, IEEE Photonics Technol. Lett. 25 (2) (2012) 107–110.
[23] Y. Kaymak, S. Fathi-Kazerooni, R. Rojas-Cessa, Indirect diffused light free-space optical communications for vehicular networks, IEEE Commun. Lett. 23 (5) (2019) 814–817.
[24] A.R. Ndjiongue, T.M. Ngatched, O.A. Dobre, H. Haas, Design of a power amplifying-RIS for free-space optical communication systems, IEEE Wirel. Commun. 28 (6) (2021) 152–159.
[25] P.K. Esubonteng, H.P.T. Nguyen, R. Rojas-Cessa, STAR: a carrier sense agnostic MAC scheme for a crowded NLoS-FSOC optical LAN, J. Opt. Commun. Netw. 14 (10) (2022) 815–827.
[26] D. Wu, Z. Ghassemlooy, H. Le Minh, S. Rajbhandari, M.-A. Khalighi, X. Tang, Optimisation of lambertian order for indoor non-directed optical wireless communication, in: 2012 1st IEEE International Conference on Communications in China Workshops (ICCC), IEEE, 2012, pp. 43–48.
[27] M. Janecek, W.W. Moses, Optical reflectance measurements for commonly used reflectors, IEEE Trans. Nucl. Sci. 55 (4) (2008) 2432–2437.
[28] M. Janecek, Reflectivity spectra for commonly used reflectors, IEEE Trans. Nucl. Sci. 59 (3) (2012) 490–497.
[29] K. Liu, J.K.Y. Ng, V.C.S. Lee, S.H. Son, I. Stojmenovic, Cooperative data scheduling in hybrid vehicular ad hoc networks: VANET as a software defined network, IEEE/ACM Trans. Netw. 24 (3) (2015) 1759–1773.
[30] X. Huang, R. Yu, J. Kang, Y. He, Y. Zhang, Exploring mobile edge computing for 5G-enabled software defined vehicular networks, IEEE Wirel. Commun. 24 (6) (2017) 55–63.
[31] X. Ge, Z. Li, S. Li, 5G software defined vehicular networks, IEEE Commun. Mag. 55 (7) (2017) 87–93.
[32] C. Masterson, Massive MIMO and beamforming: the signal processing behind the 5G buzzwords, in: 10 Massive MIMO and Beamforming: The Signal Processing behind the 5G Buzzwords, 2017, p. 10.
[33] V. Arun, H. Balakrishnan, RFocus: Beamforming using thousands of passive antennas, in: 17th $\{USENIX\}$ Symposium on Networked Systems Design and Implementation ($\{NSDI\}$ 20), 2020, pp. 1047–1061.
[34] B. Zheng, R. Zhang, Intelligent reflecting surface-enhanced OFDM: Channel estimation and reflection optimization, IEEE Wirel. Commun. Lett. 9 (4) (2019) 518–522.
[35] P.K. Esubonteng, R. Rojas-Cessa, Orientation of a diffuse reflector for improved coverage in ID-FSOC for vehicular communications, Veh. Commun. 36 (2022) 100493.
[36] N. Shlezinger, G.C. Alexandropoulos, M.F. Imani, Y.C. Eldar, D.R. Smith, Dynamic metasurface antennas for 6g extreme massive MIMO communications, IEEE Wirel. Commun. 28 (2) (2021) 106–113.
[37] R.C. Short, M.A. Cosgrove, D.L. Clark, P.J. Oleski, Performance of a demonstration system for simultaneous laser beacon tracking and low-data-rate optical communications with multiple platforms, in: Free-Space Laser Communication Technologies III, Vol. 1417, International Society for Optics and Photonics, 1991, pp. 464–475.
[38] M. Toyoshima, N. Miyashita, Y. Takayama, H. Kunimori, S. Kimura, System analysis of non-mechanical compact optical transceiver for wireless communications with a VCSEL array, in: 2008 6th International Symposium on Communication Systems, Networks and Digital Signal Processing, IEEE, 2008, pp. 187–190.
[39] G. Yun, M. Kavehrad, Indoor infrared wireless communications using spot diffusing and fly-eye receivers, Canad. J. Electr. Comput. Eng. 18 (4) (1993) 151–157.
[40] J.B. Carruthers, J.M. Kahn, Modeling of nondirected wireless infrared channels, IEEE Trans. Commun. 45 (10) (1997) 1260–1268.
[41] V. Pohl, V. Jungnickel, C. Von Helmolt, A channel model for wireless infrared communication, in: 11th IEEE International Symposium on Personal Indoor and Mobile Radio Communications. PIMRC 2000. Proceedings (Cat. No. 00TH8525), Vol. 1, IEEE, 2000, pp. 297–303.
[42] N. Hayasaka, T. Ito, Channel modeling of nondirected wireless infrared indoor diffuse link, Electron. Commun. Jpn. (Part I: Commun.) 90 (6) (2007) 9–19.
[43] C.B. Liu, B. Sadeghi, E.W. Knightly, Enabling vehicular visible light communication (V2LC) networks, in: Proceedings of the Eighth ACM International Workshop on Vehicular Inter-Networking, 2011, pp. 41–50.
[44] D.-R. Kim, S.-H. Yang, H.-S. Kim, Y.-H. Son, S.-K. Han, Outdoor visible light communication for inter-vehicle communication using controller area network, in: 2012 Fourth International Conference on Communications and Electronics (ICCE), IEEE, 2012, pp. 31–34.
[45] I. Takai, T. Harada, M. Andoh, K. Yasutomi, K. Kagawa, S. Kawahito, Optical vehicle-to-vehicle communication system using LED transmitter and camera receiver, IEEE Photonics J. 6 (5) (2014) 1–14.
[46] B. Turan, S. Ucar, Vehicular visible light communications, Visible Light Commun. (2017) 133.
[47] M. Elamassie, M. Karbalayghareh, F. Miramirkhani, R.C. Kizilirmak, M. Uysal, Effect of fog and rain on the performance of vehicular visible light communications, in: 2018 IEEE 87th Vehicular Technology Conference (VTC Spring), IEEE, 2018, pp. 1–6.
[48] M. Vieira, M. Vieira, P. Louro, P. Vieira, Vehicular visible light communication: a road-to-vehicle proof of concept, in: Optical Sensing and Detection V, Vol. 10680, International Society for Optics and Photonics, 2018, p. 106800J.
[49] D.F. Wilkins, Optical communications and obstacle sensing for autonomous vehicles, 2015, US Patent App. 14/034, 130.
[50] N. Macaluso, R. Rojas-Cessa, M. Meo, Media access schemes for indirect diffused free-space optical networks, in: 2019 IEEE 40th Sarnoff Symposium, IEEE, 2019, pp. 1–6.
[51] Y.-C. Liang, R. Long, Q. Zhang, J. Chen, H.V. Cheng, H. Guo, Large intelligent surface/antennas (LISA): Making reflective radios smart, 2019.
[52] Q. Zhang, Y.-C. Liang, H.V. Poor, Reconfigurable intelligent surface assisted MIMO symbiotic radio networks, 2020, ArXiv E-Prints.
[53] K. Liu, Z. Zhang, L. Dai, S. Xu, F. Yang, Active reconfigurable intelligent surface: Fully-connected or sub-connected? IEEE Commun. Lett. (2021).
[54] J. Chan, C. Zheng, X. Zhou, 3D printing your wireless coverage, in: Proceedings of the 2nd International Workshop on Hot Topics in Wireless, 2015, pp. 1–5.

[55] X. Xiong, J. Chan, E. Yu, N. Kumari, A.A. Sani, C. Zheng, X. Zhou, Customizing indoor wireless coverage via 3D-fabricated reflectors, in: Proceedings of the 4th ACM International Conference on Systems for Energy-Efficient Built Environments, 2017, pp. 1–10.
[56] Q. Wu, R. Zhang, Intelligent reflecting surface enhanced wireless network via joint active and passive beamforming, IEEE Trans. Wirel. Commun. 18 (11) (2019) 5394–5409.
[57] Y.-X. Ren, R.-D. Lu, L. Gong, Tailoring light with a digital micromirror device, Ann. Phys. 527 (7–8) (2015) 447–470.
[58] K.O. Odeyemi, P.A. Owolawi, O.O. Olakanmi, Performance analysis of reconfigurable intelligent surface assisted underwater optical communication system, Prog. Electromagn. Res. M 98 (2020) 101–111.
[59] V.K. Chapala, S.M. Zafaruddin, Unified performance analysis of reconfigurable intelligent surface empowered free space optical communications, 2021.
[60] M. Toyoshima, Y. Munemasa, H. Takenaka, Y. Takayama, Y. Koyama, H. Kunimori, T. Kubooka, K. Suzuki, S. Yamamoto, S. Taira, et al., Terrestrial free-space optical communications network testbed: INNOVA, in: Proc. of International Conference on Space Optical Systems and Applications (ICSOS), 2014.
[61] P. Grenfell, A. Aguilar, K. Cahoy, M. Long, Pointing, acquisition, and tracking for small satellite laser communications, in: 32nd Annual AIAA/USU Conference on Small Satellites, 2018.
[62] J.J. Gray, Johann Heinrich Lambert, mathematician and scientist, 1728–1777, Hist. Math. 5 (1) (1978) 13–41.
[63] A.K. Majumdar, J.C. Ricklin, Effects of the atmospheric channel on free-space laser communications, in: Free-Space Laser Communications V, Vol. 5892, International Society for Optics and Photonics, 2005, p. 58920K.
[64] G.-Y. Hu, C.-Y. Chen, Z.-Q. Chen, Free-space optical communication using visible light, J. Zhejiang Univ.-Sci. A 8 (2) (2007) 186–191.
[65] I.I. Kim, B. McArthur, E.J. Korevaar, Comparison of laser beam propagation at 785 nm and 1550 nm in fog and haze for optical wireless communications, in: Optical Wireless Communications III, Vol. 4214, International Society for Optics and Photonics, 2001, pp. 26–37.
[66] A.G. Alkholidi, K.S. Altowij, Free space optical communications—Theory and practices, Contemp. Issues Wirel. Commun. (2014) 159–212.
[67] Accuflect IR infrared reflectors, 2013, [Online]. Available: http://accuratus.com/accuflir.html.
[68] Thorlabs NIR bandpass and laser line filters: 700 - 1650 nm center wavelength, 2018, [Online]. Available: https://www.thorlabs.com/newgrouppage9.cfm?objectgroup_id=1000.
[69] R. Yin, Z. Ghassemlooy, E. Eso, L. Liu, An energy-efficient recovery algorithm for the free space optical communications network via reflections, Optik 241 (2021) 167045.

Paa Kwesi Esubonteng received a B.Sc. in Computer Science in 2007 at Kwame Nkrumah University of Science and Technology, M.S. and Ph.D. in Telecommunication Engineer and Electrical Engineering at New Jersey Institute of Technology (NJIT) in 2013 and 2022, respectively. His research interests are in expanding optical wireless communication using diffuse reflectors in indoor and outdoor environment, and the design of medium access control for wireless networks to provide reliable communications for emergency services. He has over 10 years of work experience in the telecommunications industry. Currently, he works as a radio engineer on Public and Life Safety Projects in New York and New Jersey.

Roberto Rojas-Cessa received the B.S. degree from Universidad Veracruzana, Mexico, a M.S. degree from Research and Advanced Studies Center, Mexico, and M.S. and Ph.D. degrees in computer and electrical engineering, respectively from Polytechnic University (currently, the New York University Tandon School of Engineering, Polytechnic Institute), Brooklyn, NY, USA. He is currently a Professor with the Department of Electrical and Computer Engineering, New Jersey Institute of Technology (NJIT). He has authored the books "Advanced Internet Protocols, Services, and Applications", (Wiley, 2012) and "Interconnections for Computer Communications and Packet Networks" (CRC Press, 2017). His research interest includes the wide area of networking, cyber–physical systems, energy, intelligent systems and learning, and emergency communications and systems. He serves in different capacities for IEEE conferences and specialized journals as reviewer and editor, and as a Panelist for U.S. National Science Foundation and U.S. Department of Energy. He was the General Chair of IEEE Sarnoff Symposium 2011 and IEEE International Conference on High Performance Switching and Routing 2020. In addition, he has been a Technical Program Committee Chair of the two flagship conferences of the Communications Society: International Conference on Communications (ICC) and Global Communications (Globecom). He is a recipient of the Excellence in Teaching Award from the Newark College of Engineering at NJIT and the New Jersey Inventors Hall of Fame–Innovators Award in 2013. He was an Invited Fellow of the Japanese Society for the Advancement of Science in 2009. He was the recipient of the Excellence Progress in Research by the Dept. of Electrical and Computer Engineering (2005).